HHS Public Access

Fetal QT Interval Estimation Using Sequential Hypothesis Testing

Suhong Yu,

Department of Radiation Oncology, University of Rochester Medical Center, 601 Elmwood Ave Box 647, Rochester, NY 14624

Barry D. Van Veen [Fellow, IEEE],

Department of Electrical and Computer Engineering, University of Wisconsin-Madison, Madison, WI 53706 USA

William J. Lutter, and

Department of Medical Physics, University of Wisconsin-Madison, Madison WI 53705 USA

Ronald T. Wakai[*]

Department of Medical Physics, University of Wisconsin-Madison, Madison WI 53705 USA

Abstract

Objective—Recent studies utilizing fetal magnetocardiography have demonstrated the efficacy of corrected QT interval (QTc) measurement for in utero diagnosis and prognosis of long QT syndrome, a leading cause of sudden death in early life. The objective of the study was to formulate and test a novel statistical estimation method to detect the end of the fetal T-wave and thereby improve the accuracy of fetal QT interval measurement.

Methods—To detect the end of the T-wave we apply a sequential composite hypothesis test to decide when the T-wave has returned to baseline. The method uses the generalized likelihood ratio test in conjunction with a low-rank spatiotemporal model that exploits the repetitive nature of cardiac signals. The unknown model parameters are determined using maximum likelihood estimation.

Results—In realistic simulations, the detector was shown to be accurate to within 10 ms (95% prediction interval), even at noise-to-signal ratios as high as 6. When applied to real data from normal fetuses, the detector agreed well with measurements made by cardiologists (−1.4 ± 6.9 ms).

Conclusions—The method was effective and practical. Detector performance was excellent despite the continual presence of strong maternal interference.

Significance—This detector serves as a valuable adjunct to traditional measurement based on subjective assessment.

rtwakai@wisc.edu.

yusuhong@gmail.com, vanveen@engr.wisc.edu

Keywords

QT interval; T-wave end; repolarization abnormalities; fetal magnetocardiography; maximum likelihood estimation; generalized likelihood ratio

I. Introduction

THE heart rate-corrected QT interval, QTc, is among the most important cardiac parameters of well-being. QTc prolongation is common in a number of serious medical conditions, including cardiomyopathy, coronary artery disease, diabetes, hypothyroidism, and a host of ion channelopathies [1], [2], [3]. In recent years, QTc has received increased attention because many drugs have been found to lengthen QTc, increasing the risk of malignant arrhythmias. The Food and Drug Administration now requires nearly all pharmaceuticals to be evaluated for their effect on QTc [4]. In addition, ion channelopathies have become an area of intense research due to rapid advances in genetic testing. QTc prolongation is a defining characteristic of most ion channelopathies, such as long QT syndrome (LQTS), and is associated with increased risk of sudden death [5].

The QT interval is defined as the time from the beginning of the QRS complex to the end of the T-wave. While the beginning of the QRS complex can be precisely resolved due to the high amplitude and abrupt onset of the QRS complex, the end of the T-wave is often ambiguous because it is gradual and easily obscured by interference and noise. Various methods have been proposed to automatically detect the T-wave end in the ECG. These include methods based estimation of the amplitude [6] and first-derivative [7] of the T-wave termination, the T-waveform area under a sliding window [8], wavelet transformations [9], and mathematical models of the T-wave [10]. Detection based on assessment of the first derivative appears to have achieved the most popularity [7], [11]. This method assumes that the derivative is non-zero in the presence of and zero in the absence of the T-wave. It has been applied to automatically detect the T-wave end and measure the QT interval of each beat.

The QT interval has been investigated far less in the fetus than in the adult due to the inability to reliably record the fetal ECG; however, recent studies utilizing fetal magnetocardiography (fMCG) have demonstrated the efficacy of the QT interval for in utero diagnosis and prognosis of LQTS [12]. Cuneo and co-workers showed that fetal QTc > 490 ms diagnosed fetal LQTS with 89% accuracy and 89% specificity, and that fetal QTc> 620 ms predicted Torsade des Pointes. Furthermore, they showed that Torsade des Pointes could be effectively treated in utero using anti-arrhythmic drugs. The significance of these findings is underscored by recent evidence that LQTS accounts for approximately 10% of unexplained fetal demise [13]. This implies that the ability to diagnose and treat LQTS in utero can save many lives.

Assessment of QTc is considerably more difficult in the fetus than in the adult. Not only is the overall amplitude of the fMCG much smaller than that of the postnatal MCG, the T-waves are noticeably flatter, having lower T/QRS amplitude ratios and more gradual terminations than T-waves after birth. Assessment of fetal QTc is further confounded by

interference from the maternal MCG and other forms of biological and environmental interference. Lastly, the amplitude of the fMCG is a strong function of gestational age, and becomes vanishingly small at gestational ages earlier than about 18 weeks.

In this paper, we present a novel statistical estimation method to detect the end of the fetal T-wave and thereby improve the accuracy of fetal QT interval measurement. Whereas automated measurement of the adult QT interval is largely a matter of convenience, the difficulty of measuring the fetal QT interval makes an automated detector a virtual necessity. Our method utilizes the generalized likelihood ratio test (GLRT) in conjunction with a spatiotemporal model that exploits the repetitive nature of cardiac signals and the considerable spatial information available in large sensor array recordings to achieve optimal performance. In section II, we motivate and describe the use of the GLRT for this application. In section III, we summarize the results of several assessments of detector performance. The performance of the detector is evaluated on simulated data and real patient data. In Section IV, we identify key attributes of the method that make it well suited for fetal application. Superscripts T and −1 denote matrix transpose and inverse, respectively, while boldface type represents matrices.

II. Methods

We approach T-wave termination estimation as a sequential composite hypothesis test. The test is sequential because we use a series of sample-by-sample tests to decide when the T-wave has returned to baseline. The test is composite because parameters such as the T-wave shape are unknown. Optimal procedures generally do not exist for composite hypothesis tests [14], so we use the generalized likelihood ratio test (GLRT). The GLRT performs hypothesis testing using a likelihood ratio in which unknown parameters are replaced by their maximum likelihood estimates (MLE). The asymptotic or large data record performance of the GLRT is known [14]. MLE has been applied to estimation of evoked responses in electro- and magneto-encephalography (EEG / MEG) [15], [16]. In particular, we have previously shown that MLE is effective at estimating spatially low rank, low bandwidth, repeated MEG signals [17] while the GLRT is effective at detecting the presence of T-wave alternans [18]. The present approach is motivated by the success of these prior formulations.

A. T-wave Termination Detection Based On a Sequential Hypothesis Test

We assume that the T-wave is locally smooth, and can be approximated as linear over a small time window of N time samples. We assume N is odd for notational convenience. A line with N uniformly-spaced points may be represented using the rows of the matrix

$$\mathbf{C}^T \;=\; \begin{bmatrix} 1 & \dots & 1 & 1 & 1 & \dots & 1 \\ -(N-1)/2 & \dots & -1 & 0 & 1 & \dots & (N-1)/2 \end{bmatrix}$$

That is, a vector of values representing uniformly-spaced values of a line with an intercept a and slope b may be expressed as:

$$[a \quad b] \, \mathbf{C}^T \quad (1)$$

We assume the temporal shape of the T-wave in the vicinity of the current sample is described by Eq. 1. Furthermore, we assume there are M spatial channels and that the T-wave lies in a rank P spatial subspace spanned by the P columns of the M-by-P matrix $\mathbf{H}$. If we assume that the T-wave in each spatial component is approximately linear, then a space-time model for N samples of the jth beat (epoch) of the measured data in the window under consideration is analogous to [17], [18]:

$$\mathbf{X}_j \;=\; \mathbf{H}\boldsymbol{\Theta}\mathbf{C}^\mathbf{T} + \mathbf{N_j} \quad (2)$$

Here $\mathbf{N}_j$ is an $M \times N$ matrix of N noise samples in the time window. The noise is assumed to be temporally white (independent from sample to sample) and Gaussian distributed with unknown spatial covariance matrix $\mathbf{R}$. The P-by-2 matrix $\boldsymbol{\Theta}$ contains intercept and slope parameters for each spatial component in the first and second columns, respectively. Concatenating all the J epochs for analysis of a length-N time window gives the model for the M-by-JN measured data as

$$\mathbf{X} \;=\; [\mathbf{X}_1 \quad \mathbf{X}_2 \dots \mathbf{X}_J] \;=\; \mathbf{H}\boldsymbol{\Theta}\mathbf{D}^\mathbf{T} + \mathbf{N} \quad (3)$$

where $\mathbf{D}^T = [\mathbf{C}^T \mathbf{C}^T \dots \mathbf{C}^T]$ is 2-by-JN.

T-wave termination is determined by sliding the length N data window $\mathbf{X}$ through the post QRS interval until we detect a return to baseline. That is, until $\boldsymbol{\Theta} = \mathbf{0}$. Hence, we define the null hypothesis as the presence of non zero slope and/or intercept.

$$H_0 : \boldsymbol{\Theta} \neq \mathbf{0} ; \mathbf{H_1} : \boldsymbol{\Theta} \;= \mathbf{0}; \quad (4)$$

Define $\mathbf{X}(k)$ as the length N segment of the measured data for post QRS time samples k, $k+1, \dots, k+N-1$. The end of the T-wave is declared (H_1) when the generalized likelihood ratio $\ell(k)$ exceeds a threshold r, that is

$$\ell(k) \;=\; \frac{p_{H_1}\left(\mathbf{X}(k); \hat{\mathbf{H}}, \hat{\boldsymbol{\Theta}}, \hat{\mathbf{R}}_1\right)}{p_{H_0}\left(\mathbf{X}(k); \hat{\mathbf{H}}, \hat{\boldsymbol{\Theta}}, \hat{\mathbf{R}}_0\right)} > r \quad (5)$$

where $p_{H_i}(.)$ denotes the probability density function (PDF) of the data under hypothesis H_i. The symbols $\hat{\mathbf{R}}_i$ denote the MLEs of the noise covariance estimated under hypothesis H_i. The PDF of the data under hypothesis H_0 is expressed as

$$p_{H_0}\left(\mathbf{X}\left(k\right);,\mathbf{H},\mathbf{\Theta},\mathbf{R_0}\right) = (2\pi)^{-MNJ/2}(\det\mathbf{R_0})^{-NJ/2}$$
$$\exp\left\{-\tfrac{1}{2}\mathrm{tr}\left[\mathbf{R_0}^{-1}\left(\mathbf{X}\left(k\right)-\mathbf{H\Theta D^T}\right)\left(\mathbf{X}\left(k\right)-\mathbf{H\Theta D^T}\right)^T\right]\right\} \quad (6)$$

where $\mathbf{R}_0$, the spatial covariance matrix of the noise, is unknown. The MLEs for the unknown noise covariance and T-wave parameters under H_0 are well-known [15], [16], [17], [18], [19]. The MLE for $\mathbf{R}_0$ is expressed as a function of the unknown $\hat{\mathbf{H}}$ and $\hat{\mathbf{\Theta}}$

$$\hat{\mathbf{R}}_0 = \frac{1}{NJ}\left(\mathbf{X}\left(k\right)-\hat{\mathbf{H}}\hat{\mathbf{\Theta}}\mathbf{C}^T\right)\left(\mathbf{X}\left(k\right)-\hat{\mathbf{H}}\hat{\mathbf{\Theta}}\mathbf{C}^T\right)^T \quad (7)$$

Substitution of $\hat{\mathbf{R}}_0$ into the PDF reveals that the MLEs $\hat{\mathbf{H}}$ and $\hat{\mathbf{\Theta}}$ are obtained by minimizing the determinant of the $\hat{\mathbf{R}}_0$ as shown in [18].

Under hypothesis H_1, since $\mathbf{\Theta} = 0$, the respective PDF is simply:

$$p_{H_1}\left(\mathbf{X}\left(k\right);\mathbf{R_1}\right) = (2\pi)^{-MNJ/2}(\det\mathbf{R_1})^{-NJ/2}$$
$$\exp\left\{-\tfrac{1}{2}\mathrm{tr}\left(\mathbf{R_1}^{-1}\mathbf{X}\left(k\right)\mathbf{X}^T\left(k\right)\right)\right\} \quad (8)$$

with

$$\hat{\mathbf{R}}_1 = \frac{1}{NJ}\mathbf{X}\left(k\right)\mathbf{X}(k)^T \quad (9)$$

Substituting the sample covariance matrix estimates into the exponential in each probability density function results in the exponential terms being independent of the data, and the GLRT is expressed as :

$$\ell'\left(k\right) = \frac{|\hat{\mathbf{R}}_0|}{|\hat{\mathbf{R}}_1|} > r' \quad (10)$$

It can be shown that $|\hat{\mathbf{R}}_0| \leq |\hat{\mathbf{R}}_1|$ with equality when $\hat{\mathbf{\Theta}}=0$ and thus $\ell(k) \quad 1$.

We evaluated two methods of automatically determining the termination time, based on the behavior of the GLRT test statistic, $\ell(k)$, in the vicinity of the T-wave termination. The test statistic is approximately the ratio of the noise variance to the total (signal plus noise) variance. Ideally, as the T-wave terminates, the test statistic increases rapidly and approaches unity at the termination; however, noise and interference within the signal subspace or temporal smearing of the signal due to bandpass filtering can cause the test statistic to peak at less than unity. Typically, the termination of the T-wave is seen to coincide with a local minimum in the second derivative of the test statistic around the time that the test statistic is

near its maximum; however, several local minima of the second derivative may be present in the vicinity of the termination. We therefore evaluated two methods of selecting local minima of the second derivative: 1) the one corresponding to the largest test statistic value and 2) the one corresponding to the minimum product of the the second derivative and the test statistic. Both methods bias the detector toward second derivative minima corresponding to higher values of the test statistic. The methods were compared using synthetic data.

B. Synthetic data

The sets of synthetic data were comprised of three components: fetal MCG signal, maternal MCG interference, and white noise. The fetal signal and maternal interference were based on templates of fMCG and maternal MCG waveforms obtained from real data with very high SNR and a well-defined fetal QT interval (Fig.1a). To model the spatial variation of the fMCG signal, we assumed it arose from a current dipole source located below the sensor array. The forward solution for a current dipole source in a half-plane was used to scale the template according to the position and orientation of each channel. The positions and orientations of the 21 channels corresponded to those of a Tristan 624 Biomagnetometer (Tristan Technologies, Inc., San Diego), which is the only fMCG device with FDA clearance. The dipole was located 0.12 m below the center channel, and was offset laterally 0.05 m in order to produce a realistic, nonsymmetrical topography. The maximum-to-mean amplitude ratio was 3. The maternal MCG, which typically shows low spatial variation, was assumed to be spatially uniform. For each channel, a 100 s time series with sampling period 1 ms was generated by replicating the fetal template 238 times at intervals of 0.42 s. The maternal QRS complexes had variable RR interval with mean 0.7 s and standard deviation 0.02 s. The signals were filtered using a 1-30 Hz passband. We also simulated the data with 0.3 Hz baseline wander, and this case was filtered using a 0.2-30 Hz pass-band. These passbands are narrower than the 1-100 Hz bandwidth typically used to record the ECG, but are appropriate here because the T-wave has much lower bandwidth than the other ECG components.

We assessed detector performance as a function of white noise amplitude for various levels of maternal interference. The white noise-to-fetal signal ratio (N/F) was defined as the root-mean square amplitude of the white noise with respect to the fetal T-wave amplitude. The maternal-to-fetal QRS ratio (M/F) was defined as the amplitude of the maternal QRS complex with respect to the fetal QRS complex in the channel with largest fetal signal. The simulation was performed 350 times, regenerating the white noise between repetitions.

We also investigated the effect of two types of interference designed to mimic maternal breathing artifacts: sinusoidal signal amplitude modulation and sinusoidal baseline wander [20]. These interferences were based on a sine wave of frequency 0.3 Hz, the approximate frequency of maternal breathing. The amplitude ratios of the baseline wander with respect to the fetal T-wave in the channel with largest fetal signal ranged from 10 to 120. The percent signal amplitude modulation ranged from 10 to 90. Various levels of white noise-to-fetal signal ratio were used. The maternal-to-fetal QRS ratio was 3.

The search for the T-wave termination was confined to a 70 ms interval, approximately centered about the ground truth termination time. The test statistic was computed every 2.5 ms, using data in a 5 ms (5-point) time window.

The second order derivatives were approximated by the second order difference, using a 2nd order central difference approximation.

C. Real data

We further evaluated the detector performance by applying it to 21 normal subjects at gestational ages 21.3-37.4 weeks, studied in a total of 30 sessions (Appendix I). The fMCG data for these patients was recorded with a 37-channel (Magnes, 4D Neuroimaging, Inc., San Diego, CA, USA) or 21-channel (Tristan 624 Biomagnetometer, Tristan Technologies, San Diego) SQUID magnetometer. At least twenty minutes of data were taken from each subject. The detector was applied to a segment of the recording, during which the fetal heart rate was stable and near baseline. On average, the segment was 67 s in length. The T-wave termination time determined by the detector was compared with that determined by a fetal cardiologist based on an averaged waveform computed from the same data. We further evaluated the detector performance by applying it to two fetuses with LQTS who showed QTc prolongation. The same procedures were used. The mother of one of these fetuses had an implantable cardioverter defibrillator (ICD) implanted above her heart that produced a large pulsation artifact. This artifact nearly obscured the fetal signal.

III. Results

Below we present results obtained using simulated and real data, and describe the behavior of the test statistic in various circumstances.

A. Synthetic data

Figure 2 shows the results of the simulations designed to determine the best method of choosing the termination time. The lowest weighted local minimum of the second derivative was clearly superior. This method was applied to obtain all subsequent results.

The main simulation results are presented in Fig. 3, which shows the mean error and standard deviation for various levels of noise and interference. In practice, the precision with which the QT interval can be estimated is approximately 10 ms. In comparison, the mean errors are relatively small. Notice, however, that the standard deviations become much larger than the mean errors as the amplitude of the noise and interference increases. In this situation, the standard deviation more accurately reflects detector performance. To attain 95% prediction interval (approximate twice the standard deviation) 10 ms, we require noise-to-signal ratio < 6, nearly independent of the level of maternal interference. In the presence of amplitude modulation, we require amplitude modulation < 30% and noise-to-signal < 5. Very high levels of baseline wander can be tolerated for noise-to-signal ratio 5.

B. Real data

For the normal subject data, the agreement between the detector and the cardiologist measurements is shown in the Bland-Altman plot and histogram in Fig. 4. The limits of agreement (1.96 * standard deviation) was 13.4 ms. Details of the normal subject results are presented in Table 1 of the Appendix. On average, the termination times determined by the detector and cardiologist differed by 1.4 ± 6.9 ms. Again, the mean error is small, and the standard deviation is a better indicator of performance. The levels of noise and maternal interference present in the real data are low compared to levels present in the simulations. Although the detector did not perform as well as would be predicted by the simulations, the performance was still excellent.

For the two fetuses with LQTS, the detector agreed with the cardiologists to within 10 ms. The detector performed well even for the case in which the recording was contaminated by large ICD artifact (Fig. 5 - 6).

IV. Discussion

In this study, we successfully demonstrated a new statistical detector that facilitates measurement of the fetal QT interval. In realistic simulations, the detector was shown to be accurate within 10 ms, even at noise-to-signal ratios as high as six. When applied to real data, the detector agreed well with measurements made by cardiologists.

A distinguishing feature of our approach is the incorporation of a low-rank spatiotemporal model which utilizes data from all of the channels to formulate a true multi-channel detector. Most prior methods have been based on detectors that operate on a single ECG lead. The multi-lead method of Laguna and coworkers, for example, performs detection on one lead at a time and then applies a detection rule to select the overall onset and end time [7]. Their method requires the use of a threshold parameter that is determined empirically, which may be problematic in cases of non-stationary noise. In our method, the unknown model parameters are determined using MLE, which also allows accurate estimation of the noise statistics. Unlike conventional whitening, which would be difficult to apply here because it requires signal-free data, MLE is able to use all of the data vectors to compute the noise covariance and thereby obtain a more stable estimate. This significantly improved detector performance. The method was applied to real data containing maternal MCG interference and performed well.

Ideally, the test statistic approaches unity at the end of the T-wave. In practice, however, residual interference and noise lying in the signal subspace may cause the test statistic to plateau at lesser values. Also, if the T-wave overlaps the P-wave of the following cycle, then the increase in the test statistic due to the termination of the T-wave may be followed by a fall due to the onset of the P-wave, resulting in a peak. In such cases it may not be possible to accurately determine the T-wave end, but the QT interval will almost certainly be prolonged. The detector still provides a lower bound on QT interval and may allow resolution of the P-wave onset, which manifests as an abrupt decrease in the test statistic.

The effectiveness of the detector is not significantly affected by morphology variation due to gestational age, disease conditions, or other factors, except that the performance is degraded by a low signal-to-noise ratio at the T-wave end due to a flat T-wave and/or low signal amplitude. The detector, however, assumes that the signal is stationary throughout the segment of data used to estimate the termination time. Fetal movement and other causes of transient morphology variation are problematic. The algorithm, therefore, should be applied during periods of fetal quiescence.

Our method can be applied to detect the onset and termination of other waveform components, such as the P-wave and QRS complex. Typically, these events can be adequately resolved using subjective assessment; however, our detector may prove useful for low SNR data, especially for determination of the P-wave onset. A modest adjustment of the spatial basis or time-window length, N, may be needed to achieve optimal performance, but in most cases the procedures implemented here for the T-wave should work well for the other components. Because the size of the fetal heart (2 cm) is smaller than the source-to-sensor distance (5-10 cm), the dipole approximation is valid. This implies that the fMCG signal should be approximately rank two, and that the signals of all of the fMCG waveform components should lie in approximately the same rank two subspace. When choosing the length of the time-window, the first requirement is that it must be sufficiently narrow that the onset/end is approximately linear within the time-window. A further consideration is the trade-off between the detectors temporal resolution and the reliability of signal estimation as the time-window length is varied.

V. Conclusion

Our method addresses a critical need for an objective and optimal means of detecting the T-wave end in fMCG data. It can serve as a valuable adjunct to subjective assessment, especially when the T-wave end is ambiguous due to low SNR.

Acknowledgments

Appendix

TABLE I

NORMAL SUBJECT DATA. GA=GESTATIONAL AGE, QRS=QRS AMPLITUDE, QRS/T=QRS/T AMPLITUDE RATIO, N/F= ROOT-MEAN-SQUARE NOISE TO FETAL QRS AMPLITUDE RATIO, M/F=MATERNAL QRS TO FETAL QRS AMPLITUDE RATIO, QT= QT INTERVAL, t_{end}= DIFFERENCE BETWEEN T-wave TERMINATION TIME FOR DETECTOR VERSUS CARDIOLOGISTS, SD=STANDARD DEVIATION

#	GA (wks)	QRS (fT)	QRS/T	N/F	M/F	QT (ms)	t_{end} (ms)
1	25.7	498	8.8	0.3	1.46	200	5.8
2	22.6	851	44.2	0.3	1.92	221	13.4
	30.4	1000	8.0	0.2	1.14	277	−13.4
	34.3	1175	7.4	0.3	1.40	296	1.9

| #	GA (wks)	QRS (fT)	QRS/T	N/F	M/F	QT (ms)	t_{end} (ms)
	37.4	1359	18.2	0.3	1.63	394	−1.9
3	37.0	3035	17.2	0.2	0.65	369	1.9
4	33.4	1170	10.0	0.3	0.91	228	−5.8
	21.6	671	18.1	0.3	1.77	223	3.8
5	26.9	977	8.1	0.3	1.62	230	−5.8
	34.1	3621	6.4	0.2	0.60	267	−3.8
6	37.0	953	9.4	1.1	1.91	234	3.8
7	28.4	4687	13.9	0.2	0.54	234	−5.7
8	21.9	790	14.8	1.6	2.76	313	−3.8
9	24.0	566	12.9	1.0	8.06	227	−9.6
	35.4	813	15.8	0.5	3.85	267	−15.4
10	24.1	1236	28.1	1.1	6.28	225	0.0
	28.9	1566	12.0	0.7	3.06	255	5.8
11	31.6	697	6.6	0.5	2.73	217	−7.7
12	30.0	692	6.9	1.1	2.67	319	1.9
13	35.0	862	10.0	0.5	4.46	246	−11.5
14	34.7	1140	10.2	1.1	1.59	250	1.9
15	35.3	2618	14.2	0.2	1.67	267	−1.9
	30.3	591	11.4	0.6	2.56	315	−1.0
16	36.3	396	8.3	0.5	6.95	243	0.5
17	33.7	3028	7.5	0.2	1.06	282	1.9
18	22.0	286	10.4	0.4	6.20	240	7.5
19	21.3	508	21.4	0.2	1.29	263	11.5
	26.4	827	13.8	0.2	1.27	254	−3.8
20	35.1	2034	16.0	0.2	1.57	200	−7.7
21	27.0	747	8.9	0.4	2.22	326	−5.8
Mean ± SD	30.1 ± 5.4	1313 ± 1055	13.3 ± 7.7	0.5 ± 0.4	2.5 ± 2.0	263 ± 47	−1.4 ± 6.9

References

[1]. Rossing P, Breum L, Major-Pedersen A, Sato A, Winding H, Pietersen A, Kastrup J, Parving HH. Prolonged qtc interval predicts mortality in patients with type 1 diabetes mellitus. Diabetic Medicine. 2001; 18(3):199–205. [PubMed: 11318840]

[2]. Bakiner O, Ertorer ME, Haydardedeoglu FE, Bozkirli E, Tutuncu B, Demirag NG. Subclinical hypothyroidism is characterized by increased qt interval dispersion among women. Medical Principles and Practice. 2008; 17(5):390–394. [PubMed: 18685279]

[3]. Lehnart SE, Ackerman MJ, Benson W, Grant AO, Groft SC, January CT, Lathrop DA, Lederer WJ, Makielski JC, Mohler PJ, Moss A, Nerbonne JM, Olson TM, Przywara DA, Towbin JA, Wang LH, Marks AR. Inherited arrhythmias - a national heart, lung, and blood institute and office of rare diseases workshop consensus report about the diagnosis, phenotyping, molecular mechanisms, and therapeutic approaches for primary cardiomyopathies of gene mutations affecting ion channel function. Circulation. 2007; 116(20):2325–2345. [PubMed: 17998470]

[4]. Darpo B. The thorough qt/qtc study 4 years after the implementation of the ich e14 guidance. British Journal of Pharmacology. 2010; 159(1):49–57. [PubMed: 19922536]

[5]. Cerrone M, Priori SG. Genetics of sudden death: focus on inherited channelopathies. European Heart Journal. 2011; 32(17):2109–U148. [PubMed: 21478491]

[6]. Mclaughlin NB, Campbell RWF, Murray A. Comparison of automatic qt measurement techniques in the normal 12-lead electrocardiogram. British Heart Journal. 1995; 74(1):84–89. [PubMed: 7662463]

[7]. Laguna P, Thakor NV, Caminal P, Jane R, Yoon HR. New algorithm for qt interval-analysis in 24-hour holter ecg - performance and applications. Medical & Biological Engineering & Computing. 1990; 28(1):67–73. [PubMed: 2325452]

[8]. Zhang QH, Manriquez AI, Medigue C, Papelier Y, Sorine M. An algorithm for robust and efficient location of t-wave ends in electrocardiograms. Ieee Transactions on Biomedical Engineering. 2006; 53(12):2544–2552. [PubMed: 17153212]

[9]. Martinez JP, Almeida R, Olmos S, Rocha AP, Laguna P. A wavelet-based ecg delineator: Evaluation on standard databases. Ieee Transactions on Biomedical Engineering. 2004; 51(4): 570–581. [PubMed: 15072211]

[10]. Vila JA, Gang Y, Presedo JMR, Fernandez-Delgado M, Barro S, Malik M. A new approach for tu complex characterization. Ieee Transactions on Biomedical Engineering. 2000; 47(6):764–772. [PubMed: 10833851]

[11]. Laguna P, Jane R, Caminal P. Automatic detection of wave boundaries in multilead ecg signals - validation with the cse database. Computers and Biomedical Research. 1994; 27(1):45–60. [PubMed: 8004942]

[12]. Cuneo BF, Strasburger JF, Yu SH, Horigome H, Hosono T, Kandori A, Wakai RT. In utero diagnosis of long qt syndrome by magnetocardiography. Circulation. 2013; 128(20):2183–2191. [PubMed: 24218437]

[13]. Crotti L, Tester DJ, White WM, Bartos DC, Insolia R, Besana A, Kunic JD, Will ML, Velasco EJ, Bair JJ, Ghidoni A, Cetin I, Van Dyke DL, Wick MJ, Brost B, Delisle BP, Facchinetti F, George AL, Schwartz PJ, Ackerman MJ. Long qt syndrome-associated mutations in intrauterine fetal death. JAMA. 2013; 309(14):1473–82. [PubMed: 23571586]

[14]. Kay, SM. Fundamentals of statistical signal processing:detection theory. Prentice-Hall PTR; 1993. p. 200-206.

[15]. Dogandzic A, Nehorai A. Estimating evoked dipole responses in unknown spatially correlated noise with eeg/meg arrays. IEEE Transactions on Signal Processing. 2000; 48(1):13–25.

[16]. Dogandzic A, Nehorai A. Generalized multivariate analysis of variance. IEEE Signal Processing Magazine. 2003; 20(5):39–54.

[17]. Baryshnikov BV, Van Veen BD, Wakai RT. Maximum-likelihood estimation of low-rank signals for multiepoch meg/eeg analysis. IEEE Transactions on Biomedical Engineering. 2004; 51(11): 1981–1993. [PubMed: 15536900]

[18]. Yu SH, Van Veen BD, Wakai RT. Detection of t-wave alternans in fetal magnetocardiography using the generalized likelihood ratio test. Ieee Transactions on Biomedical Engineering. 2013; 60(9):2393–2400. [PubMed: 23568477]

[19]. Murihead, R. Aspects of Multivariate Statistical Theory. Wiley; New York: 1982.

[20]. Porta A, Baselli G, Lombardi F, Cerutti S, Antolini R, Del Greco N, Ravelli F, Nollo G. Performance assessment of standard algorithms for dynamic r-t interval measurement: comparison between r-t-apex and r-t-end approach. Medical Biological Engineering Computing. 1998; 36(1):35–42. [PubMed: 9614746]
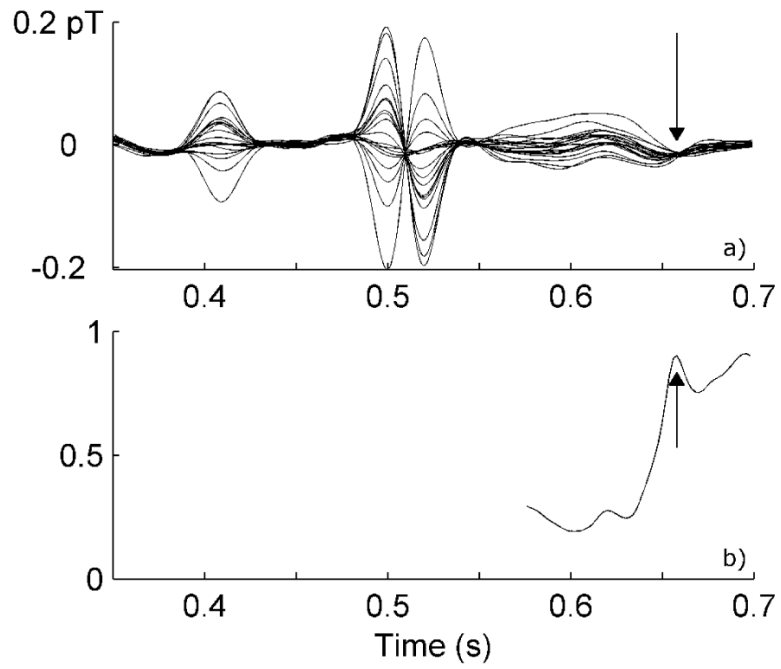
Fig. 1.
Simulation result showing a) averaged fMCG waveform and b) test statistic, $\ell'(k)$. The simulated data was formed by embedding 100 high SNR fetal templates in white noise and maternal interference. In this example, the ratio of the root-mean square (rms) amplitude of the white noise with respect to the fetal T-wave was 4. The ratio of the amplitude of the maternal QRS complex with respect to the fetal QRS complex in the channel with largest fetal signal was 1. The ground truth T-wave termination is indicated by the arrows.
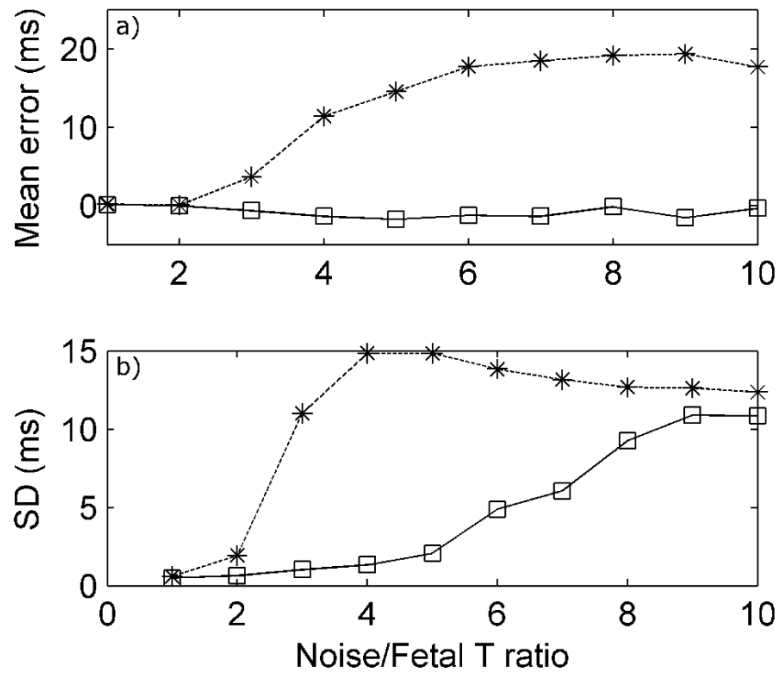
Fig. 2.
Mean detector error and standard deviation (SD) for two methods of choosing the termination time: local minimum of the second derivative with highest test statistic (asterisks) and lowest local minimum of the product of the test statistic and the second derivative (squares). The synthetic data included white noise and maternal interference. The maternal-to-fetal QRS amplitude ratio was 1. Each data point represents the accumulated result of 300 simulations
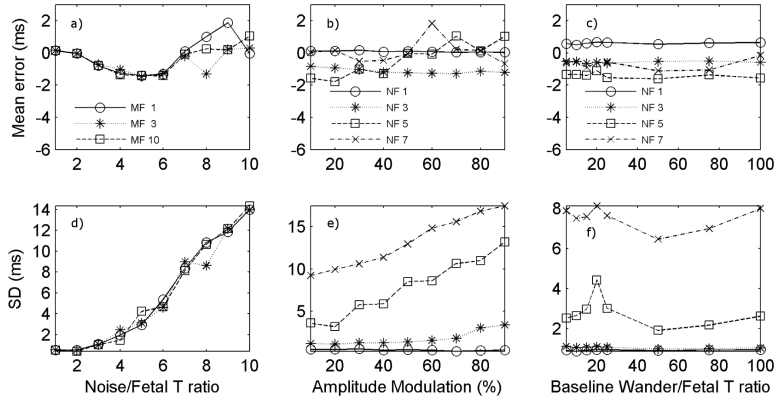
Fig. 3.
Mean detector error and standard deviation (SD) as a function of the white noise-to-fetal signal amplitude (N/F) for three levels of maternal-to-fetal QRS amplitude (M/F; a, d), the percent signal modulation for four N/F ratios (b, e), and the baseline wander amplitude for four N/F ratios (c, f). Each data point represents the accumulated result of 350 simulations.
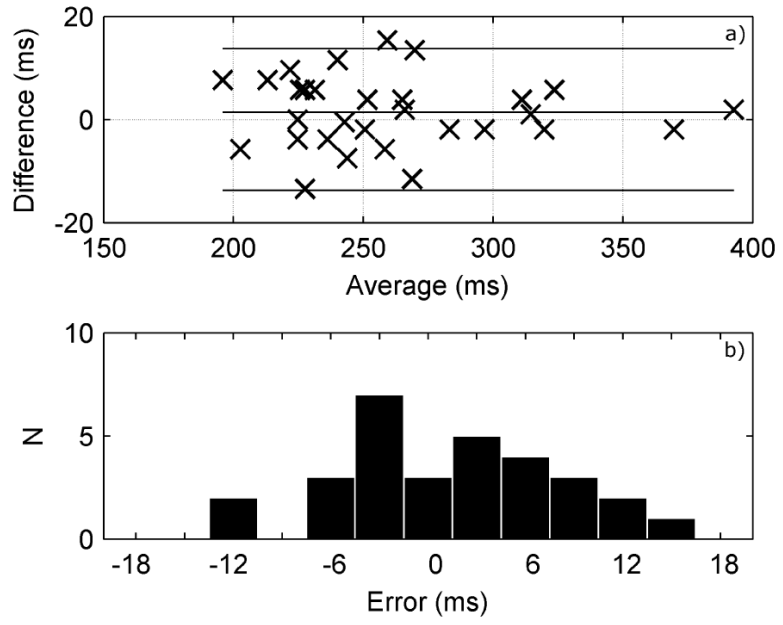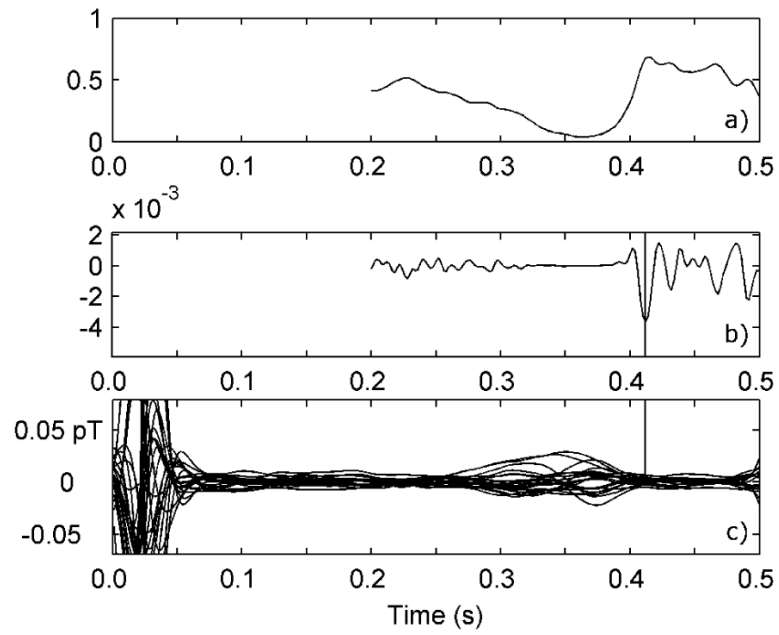
Fig. 4.
a) Bland-Altman plot showing the agreement between the detector and the cardiologist measurements of QT interval in normal subjects and b) histogram of the detector errors relative to the cardiologist measurement.
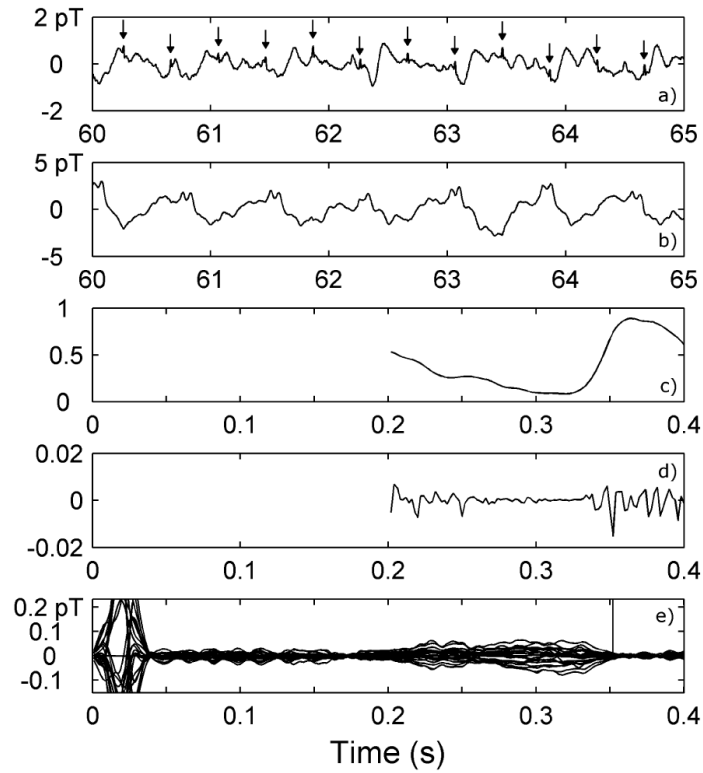
Fig. 5.
Example of fetus with long QT syndrome. a) Test statistic, b) weighted second derivative of test statistic, and c) averaged fMCG waveform, showing late-peaking T-wave typical of fetal LQTS. The termination time chosen by the cardiologist was 10 ms earlier than the time chosen by the detector (vertical line).

Fig. 6.
Example of fetus with long QT syndrome, in which QT assessment is confounded by artifact from the mothers implantable cardioverter defibrillator (ICD). a) fMCG tracing from a channel with barely visible fetal signal (arrows), b) fMCG tracing from a channel with strong, periodic pacemaker artifact, c) test statistic, d) weighted second derivative of the test statistic, e) averaged fMCG waveform where independent component analysis was used to separate the fetal signal from the interference. The termination time chosen by the cardiologist was the same as the time chosen by the detector (vertical line).